Geochemistry, Geophysics, Geosystems®

AGU ADVANCING EARTH AND SPACE SCIENCE

RESEARCH ARTICLE
10.1029/2022GC010340

Curie Temperatures and Emplacement Conditions of Pyroclastic Deposits From Popocatépetl Volcano, Mexico

K. Dudzisz[1,2], A. Kontny[1], and L. M. Alva-Valdivia[3]

[1]Karlsruhe Institute of Technology (KIT), Institute of Applied Geosciences, Karlsruhe, Germany, [2]Institute of Geophysics, Polish Academy of Sciences, Warsaw, Poland, [3]Universidad Nacional Autónoma de México (UNAM), Instituto de Geofísica, Laboratorio de Paleomagnetismo, Ciudad Universitaria, Ciudad de México, Mexico

Key Points:

- Several Curie temperatures were observed in pyroclastic deposits
- Temperature and field dependence of magnetic susceptibility are suited to separate eruption phases
- Irreversible Curie temperatures in heating and cooling curves observed in block-and-ash flows may suggest rapid quenching

Supporting Information:

Supporting Information may be found in the online version of this article.

Correspondence to:

K. Dudzisz and A. Kontny,
katarzyna.dudzisz@gmail.com;
agnes.kontny@kit.edu

Citation:

Dudzisz, K., Kontny, A., & Alva-Valdivia, L. M. (2022). Curie temperatures and emplacement conditions of pyroclastic deposits from Popocatépetl volcano, Mexico. *Geochemistry, Geophysics, Geosystems*, *23*, e2022GC010340. https://doi.org/10.1029/2022GC010340

Received 13 JAN 2022
Accepted 20 JUL 2022

Author Contributions:

Conceptualization: A. Kontny
Data curation: K. Dudzisz
Formal analysis: K. Dudzisz, A. Kontny, L. M. Alva-Valdivia
Funding acquisition: L. M. Alva-Valdivia
Investigation: K. Dudzisz, L. M. Alva-Valdivia
Methodology: K. Dudzisz, A. Kontny
Supervision: A. Kontny
Validation: K. Dudzisz
Visualization: K. Dudzisz
Writing – original draft: K. Dudzisz, A. Kontny, L. M. Alva-Valdivia

Abstract Most pyroclastic deposits of Popocatépetl volcano were emplaced at high temperatures and have similar mafic to more evolved compositions, suggesting a long-lived, interconnected magma environment. We performed a magnetic and microscopic study on different eruptive sequences <14 ky in age and found that temperature and field dependence of magnetic susceptibility are suited to separate eruption phases. We observed homogeneous titanomagnetite with Curie temperatures (T_C) of 50–200°C and 200–400°C, together with different amounts of oxy-exsolved titanomagnetite with $T_C \sim 570$°C. Some block-and-ash flow deposits show remarkably irreversible T_C in heating and cooling branches with a positive ΔT_C ($T_{C\,heating}$–$T_{C\,cooling}$) of up to 130°C in the center. The central part of this sequence is characterized by decreasing magnetic susceptibility and low field dependence of magnetic susceptibility (<10%), which is atypical for ulvöspinel-rich titanomagnetite. The nonreversibility of heating and cooling runs measured with rates of around 10 K/min is probably related to vacancy-enhanced nanoscale chemical clustering, which seems to occur preferentially during rapid quenching, possibly combined with subtle maghemitization. In contrast, pumice layers have the highest field dependence (~20%) and contain Ti-rich and intermediate titanomagnetite with $T_C < 100$ and ~300°C, which are in line with mafic and more evolved magma composition. In intermediate phases, irreversibility of T_C is more common but with a relatively low ΔT_C of ±20°C. We suggest that magneto-mineralogy in pyroclastic density currents is complex but offers a complementary tool to the paleomagnetic directional analysis for emplacement temperature and contribute information on the volcanic material history and their emplacement conditions.

Plain Language Summary Explosive eruptions of volcanoes are a dangerous threat to human settlements. In this study, we investigated pyroclastic material from the last 14 ky of Popocatépetl volcano using magnetic mineral assemblages, hysteresis properties, and temperature- and field-dependent magnetic susceptibility. The data are suited to separate different eruption phases and provide information on the volcanic material history and emplacement conditions. Magnetic susceptibility analyses are suggested to be a complementary tool to the paleomagnetic directional analysis for the determination of emplacement temperatures.

1. Introduction

Pyroclastic density currents (PDCs) represent one of the most dangerous natural hazards on Earth, and stratovolcanoes like Unzen in Japan, Mt. St. Helens in USA, and Popocatépetl in Mexico give examples of devastating events in the last millennia (e.g., Christiansen & Peterson, 1981; Siebe et al., 1996; Yamamoto et al., 1993). They originate from volcanic eruptions when mixtures of hot gases and fragmental particles (ash, lapilli, blocks, and boulders) become buoyant and move laterally (Cole et al., 2015; Lube et al., 2020). PDCs are density-stratified flows composed of a basal dense granular flow and an over-riding dilute ash cloud. The term block-and-ash flow is often used for the basal dense granular flow (e.g., Pensa et al., 2019). Given the great destructiveness posed by PDCs, the understanding of their formation mechanism and behavior is important for hazard prediction. PDCs can be characterized by multiphase flow transport regimes and gas-particle interactions, spanning from fast and high-energy surges to slow and dense flows, which produce a wide variety of deposit characteristics (e.g., Lerner et al., 2022). The Plinian eruption, for example, occurs in pulses that mostly start with minor ash falls and ash flows and reach their peak with the deposition of pumice falls, the emplacement of hot ash flows, and finally extensive mudflows (e.g., Siebe et al., 1996). Since 1994, the observed reawakening of the Popocatépetl volcano causes a threat to nearby populations as huge emissions of ash and fumarolic gases (Love et al., 1998) together with subsequent episodes of rapid dome growth at the summit crater were reported (e.g.,

Gómez-Vázquez et al., 2016). This present-day activity is associated with mild to moderately explosive Vulcanian activity, and ashfall frequently reaches Mexico City and the city of Puebla located 60 and 45 km from the volcano, respectively (Mangler et al., 2019). In the Holocene, explosive activity proceeded effusive phases of the Popocatépetl eruption that lasted around 35 years and had a significant impact on habitants in the pre-Hispanic times (Ramírez-Uribe et al., 2022).

The magnetic mineralogy of pyroclastic deposits is controlled by Fe-Ti oxides intergrown with olivine-pyroxene phenocrysts crystallized between 870 and 1,000°C in the magma chamber or subvolcanic dike intrusions (e.g., Mangler et al., 2020; Mollo et al., 2013; Sosa-Ceballos et al., 2012), Fe-Ti oxides conserved in the clasts from the volcanic dome structure before the explosive collapse (e.g., Saito et al., 2003, 2004), a juvenile component that was crystallized from lava and then quenched during eruption and deposition (e.g., Jackson & Bowles, 2014; Lied et al., 2020), and processes after the deposition, such as magma degassing, which may cause a reduction of the oxide assemblages, or fluid-induced alteration causing a low-temperature (<350°C) maghemitization (e.g., Dunlop & Özdemir, 1997; Oliva-Urcia et al., 2011). The most important magnetic minerals in volcanic rocks belong to the solid solution series of titanomagnetite ($Fe_{3-x}Ti_xO_4$) with magnetite ($x = 0$) and ulvöspinel ($x = 1$) as end-members. The chemical composition of homogeneous titanomagnetite in volcanic rocks depends on Ti/(Ti + Fe) ratio as well as oxygen fugacity and temperature of the melt. If titanomagnetite crystallizes in equilibrium with ilmenite, an increase in oxygen fugacity, as well as a decreasing Ti/(Ti + Fe) ratio, causes a decreasing ulvöspinel component in titanomagnetite (Lattard et al., 2006). Also increasing cooling rate and crystallization temperature decrease the ulvöspinel component in titanomagnetite (e.g., Mollo et al., 2013). A good proxy to evaluate titanomagnetite composition is the Curie temperature (T_C) determined from temperature-dependent magnetic susceptibility [κ(T)] measurements (e.g., Lattard et al., 2006). But magnetic properties of pyroclastic deposits are not only controlled by the titanomagnetite composition, but also by the amount of the ferrimagnetic minerals and their grain size (e.g., Dunlop & Özdemir, 1997).

Saito et al. (2003, 2004) have shown that Fe-Ti oxide minerals from block-and-ash flow deposits of the Yufo volcano, Japan, can be used to unravel the oxidation processes in the lava dome before an eruption. These authors have discriminated three different Fe-Ti oxide mineral assemblages (type A: homogeneous titanomagnetite; type B: exsolved titanomagnetite with lower ulvöspinel component and composed of two to three phases, and type C—highly oxidized up to hematite) and suggested that types B and C result from oxidation processes of type A in the outer shell of a lava dome. Outer parts of the dome, where lava intruded and caused an endogenous growth under low effusion rates, were distinguished from exogenous dome growth with high effusion rates. While the first mechanism causes higher oxidation of primarily homogeneous Fe-Ti oxides (types B and C), the latter is characterized by nonoxidized homogeneous Fe-Ti oxides (type A). These types A–C are described for pyroclastic deposits worldwide (e.g., Alva-Valdivia et al., 2019; Lerner, Cronin, & Turner, 2019; Lerner, Cronin, Turner, et al., 2019).

Emplacement temperatures of PDCs can range from cool depositions in lahars or other collapses not primarily related to an eruption (e.g., gravitational collapse triggering mudflows) to temperatures >800°C (e.g., Lerner, Cronin, Turner, et al., 2019). They can be evaluated in several ways like direct measurements of temperature-depth profiles (e.g., Banks & Hoblitt, 1996), using satellite images (Denniss et al., 1998; Wooster et al., 2000), by studying characteristic features, such as carbonized material, the reflectance of charcoal or bone fragments (Mastrolorenzo et al., 2001; Pensa et al., 2015; Sawada et al., 2000), or indirectly using paleomagnetic techniques (e.g., Alva-Valdivia et al., 2019; Paterson et al., 2010). Paleomagnetism uses a recorded magnetic signal known as thermoremanent magnetization, and emplacement temperatures of pyroclastic deposits are typically derived from oriented clasts that can originate from the magma chamber (juvenile clasts), from conduit walls (accessory clasts), or be ripped up along the flow path (accidental lithics; Alva-Valdivia et al., 2019), but also from the ash matrix (e.g., Lerner, Cronin, Turner, et al., 2019). When rocks are cooled from a temperature higher than the T_C of constituting magnetic minerals, the minerals acquire a new magnetization parallel to the Earth's magnetic field at the time of emplacement. This method can be applied up to the T_C of the constituent ferrimagnetic phase (e.g., Paterson et al., 2010; Lerner, Cronin, & Turner, 2019, Lerner, Cronin, Turner, et al., 2019). For the PDC at Mt. Taranaki, New Zealand, a hot lava dome collapse is suggested based on paleomagnetic investigations of ash and clasts (Lerner, Cronin, & Turner, 2019). Alva-Valdivia et al. (2019) have reported three emplacement temperature ranges (320–370°C, 400–460°C, and >500°C) for the phreatomagmatic Cerro Colorado tephra deposits, Mexico, and many of their κ(T) curves show significant nonreversible behavior, which may indicate different thermal

profiles due to stratigraphic variation of titanomagnetite within the PDC deposit (Bowles et al., 2018). Nonreversibility may be due to maghemitization (Oliva-Urcia et al., 2011), high-temperature nonstoichiometry (Brachfeld & Hammer, 2006), cation ordering processes below the titanomagnetite binary solvus (Jackson & Bowles, 2014), or vacancy-enhanced nanoscale chemical clustering in the octahedral sublattice (Bowles et al., 2019).

Because cation order/disorder in pure magnetite only affects the Fe^{2+} and Fe^{3+} cation distribution in the octahedral sites (tetrahedral sites only have Fe^{3+}), different quenching histories give the same T_C, and T_C from laboratory heating and cooling runs are reversible. Harrison and Putnis (1999) have shown that this is not the case for synthetic magnesioferrite ($MgFe_2O_4$) and Lattard et al. (2006) have documented thermomagnetic irreversibility for synthetic titanomagnetite ($Fe_{3-x}Ti_xO_4$). These authors suggested that either cation vacancies or interactions of magnetic and cation ordering have an influence on T_C. Jackson and Bowles (2014) documented for the first time significant nonreversibility of T_C from pumice and ash flow samples of the Mt. St. Helens volcano, USA, and first argued that this nonreversibility is related to cation ordering that might be affected by the emplacement temperature and cooling rate of volcanic sequences containing homogeneous titanomagnetite. The same group of researchers has studied the atomic-scale processes responsible for the T_C variations and suggested that vacancy-enhanced nanoscale chemical clustering on the octahedral sites within the titanomagnetite sublattice is more consistent with their X-ray magnetic circular dichroism and Mössbauer spectroscopy study (Bowles et al., 2019) than a reordering of cations. Their data also suggest that Mg substitution mainly occurs on octahedral sites, while Al substitution occurs on both octahedral and tetrahedral sites. Both cations are ubiquitous in small concentrations in magmatic titanomagnetites (e.g., Bowles et al., 2013; Lied et al., 2020; Macías et al., 2020). In addition, changes in T_C are enhanced in their studied synthetic samples by oxidation at low temperatures (150°C). Nanoscale unmixing in titanomagnetite is documented in a study by Lied et al. (2020) from pyroclastic maar deposits. After κ(T) was measured up to 700°C in argon, the nanostructures were no longer present and a homogeneous titanomagnetite was produced again with significantly lower T_C in the cooling curve compared to the heating curve. Therefore, cooling history seems to play an important role in T_C's irreversibility.

Magnetic minerals record both rock magnetic and paleomagnetic information. The aim of this study is to investigate if magnetic mineralogy is also suited to separate different eruptive sequences from PDCs. For this purpose, we measured the temperature dependence of magnetic susceptibility on four profiles comprising different eruptive sequences from the last 14 kyr of the Popocatépetl volcano to test if varying T_C can be related to the type of pyroclastic deposits. We combined our investigations with magnetic susceptibility and its field dependence and hysteresis properties as well as with magnetic mineralogy investigations through reflected light and scanning electron microscopy. This approach can be complementary to the paleomagnetic directional analysis for emplacement temperature determination and help to unravel the history of the volcanic material and its emplacement conditions.

2. Geological Setting

The Popocatépetl volcano is located in the eastern part of the Trans-Mexican Volcanic Belt, an approximately east-west-aligned zone that extends for more than 1,000 km from the Pacific coast to the Gulf of Mexico (Figure 1). The mostly calc-alkaline composition of the volcanic products results from the subduction of the Cocos plate beneath the North American plate and dacitic to andesitic volcanism occurred in the region at least since the Oligocene time and continues to present. The Popocatépetl stratovolcano lies about 70 km SE of Mexico City and is considered one of the most active volcanoes in the country (Ramírez-Uribe et al., 2022).

Current models of the plumbing system of the Popocatépetl volcanic complex suggest at least two (mafic and evolved) long-lived interconnected magmatic environments in the mid to upper crust. Mangler et al. (2020) suggest that high-Mg orthopyroxene + clinopyroxene + Cr-spinel ± sulfide crystallized from the mafic magma at 1,000–1,115°C, whereas evolved, shallower melt produced plagioclase + low-Mg orthopyroxene + clinopyroxene + Fe-Ti oxides + apatite ± sulfides at long-term storage temperatures of around 970°C. In addition, mixing and hybridization between these two magmas were described (e.g., Sosa-Ceballos et al., 2012). Lavas and pumices were fed from this reservoir documenting a range of eruption styles (effusive vs. explosive). A complex preeruptive recharge and mixing dynamic is testified by zoned pyroxene crystals of vast textural diversity (e.g., Mangler et al., 2022; Ramírez-Uribe et al., 2022). Mineral chemical studies on

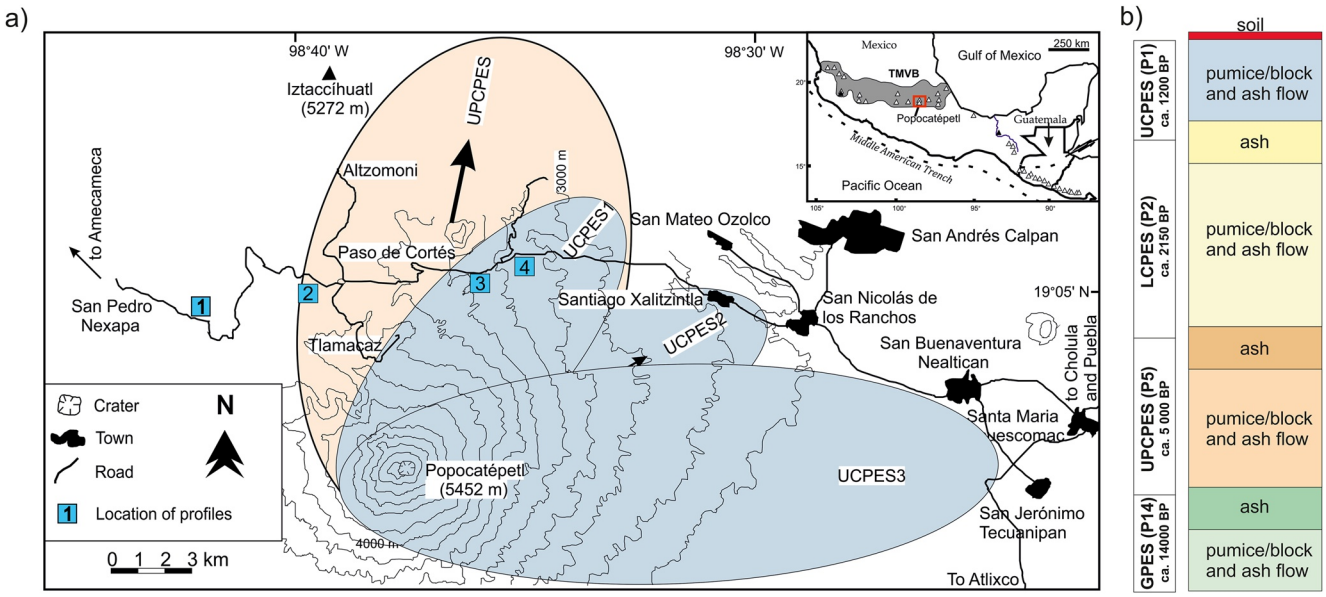

Figure 1. (a) Map of sampling site location. Shaded areas indicate areas covered by Plinian pumice-fall deposits of various ages, whereas arrows indicate dispersal directions of these deposits. (b) Simplified stratigraphic profile of the Popocatépetl deposits of the last 14,000 years (modified after Siebe and Macías (2006)). Profile 1 (POP1) at the "Christmas Tree" with the so-called "Tutti-Frutti" pumice); profile 2 was taken from Manantial; profile 3 (POP3a,b) was located between the police station at the top and La cantera de los fluchos, and profile 4 (POP4a,b,c) at La cantera de los fluchos. Abbreviations: UCPES—Upper Ceramic Plinian Eruption Sequence (ca. 1,200 years. BP); LCPES—Lower Ceramic Plinian Eruption Sequence (ca. 2,150 years. BP); UPCPES—Upper Pre-Ceramic Plinian Eruption Sequence (ca. 5,000 years. BP); GPES—Glacial Plinian Eruption Sequence (ca. 14,000 years. BP). The inset map shows the Trans Mexican Volcanic Belt; open triangles—volcanoes; solid squares—cities; red box—study area shown in the main map.

orthopyroxene in pumice from the 1,200 years BP Plinian event (named P1) record magma recharge until days before an eruption (Mangler et al., 2022).

The current volcanic structure of Popocatépetl is built on cones that were destroyed by the vast cataclysmic events when an older volcano collapsed producing a debris avalanche (Figure 1; Siebe et al., 2017). Deposits from this type are associated with Plinian eruptions at about 22,000–24,000 years BP. A further major phreato-Plinian eruption occurred about 14,000 years BP (named P14) and is associated with the emplacement of the Plinian fall deposits "Tutti-Frutti" (Siebe & Macías, 2006). These characteristic deposits are used as a stratigraphic marker in the area of Mexico City and consist mainly of two heterolithologic fall breccia, including dacitic orange pumice with granodiorite, hornfels, arenite, and xenoliths from the local basement (Siebe & Macías, 2006; see Figure 2a, profile 1, P14).

The Holocene eruptions (Figure 1) started with minor ashfall and ash flows and peaked in an episode of Plinian pumice fall, pyroclastic hot ash flows, and lahars, which mark the end of the sequence. The Upper Pre-Ceramic Plinian Eruptive Sequence (UPCPES) is the oldest of the recent Plinian eruptions (ca. 5,000 years BP) and will be referred to in our study as P5 (Siebe & Macías, 2006). According to Arana-Salinas et al. (2010), P5 is the result of three main eruptive phases, including Vulcanian eruptions producing block-and-ash flows from a growing dome, phreatomagmatic explosions triggered by water-magma interaction (surges), and Plinian eruptions with pumice and ash deposits. The Lower Ceramic Plinian Eruptive Sequence (LCPES) occurred approximately 2,150 years BP and will further be named P2. The pumice fall from both eruptions is characterized by ochre-brown andesite pumice with dark gray scoria and light green siltstone clasts (Siebe & Macías, 2006), making a distinction between P5 and P2 in the field difficult. The deposition of the Upper Ceramic Plinian Eruptive Sequence (UCPES, referred to as P1) occurred ca. 1,200 years BP and is characterized by three Plinian pulses (UCPES1-3 in Figure 1a) that led to the deposition of pink-gray andesite pumice. These different sequences (P5, P2, and P1) consist of nearly the same chemical and mineralogical andesitic composition, which suggests a long-lived magma chamber (Siebe & Macías, 2006) in line with recent petrological studies (Mangler et al., 2020, 2022; Ramírez-Uribe et al., 2022 and references therein). Examples of the sampled stratigraphic sequences associated with the most recent major Plinian eruptions at Popocatépetl are shown in Figure 2. Since the last major Plinian

10.1029/2022GC010340

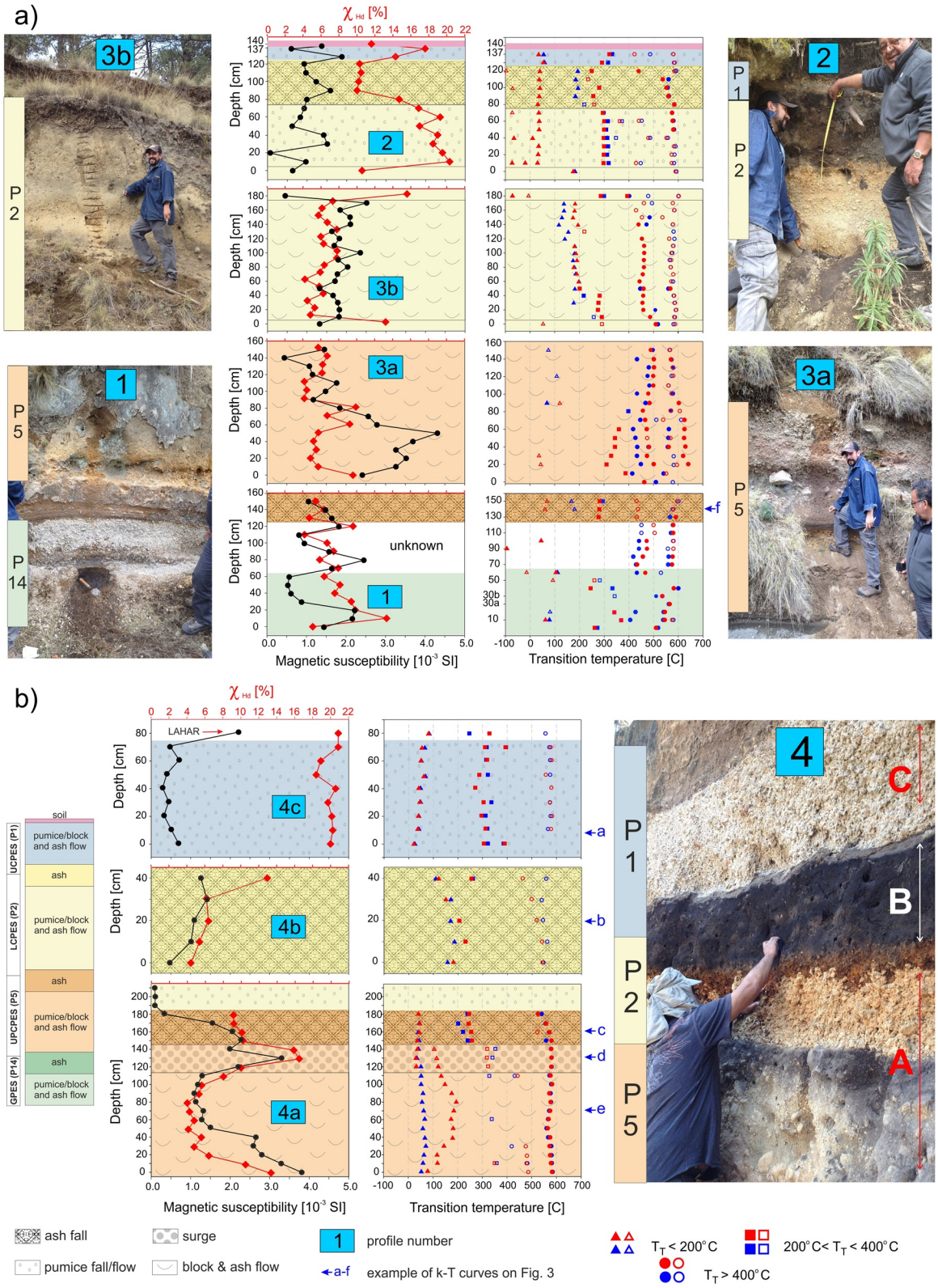

Figure 2. Changes in magnetic susceptibility (black) and field dependence (red) parameter (left column) and transition temperatures (right column) with depth for the different profiles along the Paso de Cortés road. Stratigraphic positions are shown in the field photographs and data profiles. Filled symbols in the right columns represent the transition temperatures of the dominant phase, whereas open symbols describe the minor phases derived from κ(T) curves. Red and blue indicate temperatures obtained from heating and cooling curves, respectively. The field dependence parameter (χ_{Hd}) was calculated according to Equation 1. Small blue arrows with letters (on the right) indicate the location of κ(T) curves shown in Figure 3. For an explanation of abbreviations, see Figure 1.

event about 1,200 years BP, the Popocatépetl volcano has produced only moderate eruptions. Ongoing activity, which commenced in 1994, is characterized by dome emplacement and destruction cycles that formed and destroyed 38 lava domes in 28 years so far (Gómez-Vazquez et al., 2016).

3. Materials and Methods

3.1. Field Sampling

Pumice, ash fall, and block-and-ash flow deposits of four profiles along the road Paso de Cortés, which is located between Popocatépetl in the south and Iztaccíhuatl in the north (Figure 1a), were collected in 2016. Those profiles cover eruptive sequences of P14, P5, P2, and P1 of the Popocatépetl's last 14,000 years of eruptive history, and some of the profiles were composed of different stratigraphic levels (named 4a, 4b). For all profiles, we measured magnetic susceptibility with a hand-held susceptometer (SM30) and took samples every 10 cm. The pyroclastic material (ash matrix, pumice, and lithic clasts) was scratched from the outcrop (see markings in Figure 2a) using wood or plastic spoons and transported in plastic bags. The maximum size of pumice and lithic clasts was around 2 cm in diameter, but for measurements, pieces below 0.3 cm were used. In total, we collected about 100 samples from the profiles, which had a maximum length of approximately 2 m.

3.2. Optical Microscopy and SEM

From the whole collection, we prepared 37 polished thin sections for transmitted and reflected light investigations. Microscopic observations were performed with a Leitz Orthoplan polarizing microscope. To better characterize magnetic mineral assemblages under reflected light, ferrofluid and oil immersion were used. Scanning electron microscopy (SEM) with back-scattered electron (BSE) imaging was combined with EDX to obtain also information on the qualitative mineral chemical composition of the Fe-Ti oxides assemblages. The carbon-coated polished thin sections were investigated with an FEI Quanta 650 FEG ESEM with an accelerating voltage of 15 kV and a working distance of 10 mm at the Laboratory for Electron Microscopy at KIT.

3.3. Magnetic Experiments

Bulk magnetic susceptibility was measured for all profiles in situ with a hand-held susceptometer (SM30) and then for each sample with a KLY-4S Kappabridge (Agico) in the laboratory. This instrument coupled with a CS-2 furnace was also used for the temperature-dependent magnetic susceptibility [κ(T)] measurements in the temperature range from −192°C or room temperature to 700°C to determine possible changes in magnetic mineralogy. The high-temperature heating and cooling runs were measured in an inert argon atmosphere to prevent oxidation during the measurement. Curie temperature was estimated based on the peak-tangent method proposed by Lied et al. (2020; an example is given in Figure S4 in Supporting Information S1) and is further called transition temperature. The difference between values obtained from heating and cooling curves is given as ΔT_C. Field dependence of the magnetic susceptibility was measured using the Kappabridge (KLY-4S) in the field range between 2 and 450 A/m and then normalized by mass. The field dependence parameter (χ_{Hd}) was calculated according to de Wall (2000):

$$\chi_{Hd}\,[\%] = [(k300 - k30)/k300] \times 100 \quad (1)$$

where k300 and k30 are magnetic susceptibility measured at 300 and 30 A/m, respectively.

Hysteresis parameters were measured using an AGFM Micromag 2,900 apparatus in fields up to 1.2 T. The IRM curves were analyzed using the component analysis by Maxbauer et al. (2016). Three parameters describe the magnetic components obtained from the statistical analysis: SIRM proportional to the mineral content in the sample, the mean coercivity (B1/2) at which half of the SIRM is reached, and the dispersion parameter (DP) corresponding to the individual cumulative log-normal distribution. All measurements were made at the Institute of Applied Geoscience, KIT, except for hysteresis data that were measured at the paleomagnetic laboratory of the Geophysics Institute at UNAM.

4. Results

4.1. Magnetic Properties

Depth distribution of magnetic susceptibility (κ) and its field dependence (χ_{Hd}), as well as transition temperatures from κ(T) curves along all studied profiles, is shown in Figure 2. Both magnetic susceptibility measured in the field and the laboratory display approximately the same trend; thus, only the field measurements are shown (in black). Magnetic susceptibility values show a large variation but do not exceed 5×10^{-3}SI. The lowest values of κ correlate with the highest values of χ_{Hd} reaching up to 20% and are observed especially in pumice-fall deposits of P1 and P2 (Figure 2; profiles 2 and 4c). For most of the other deposits, the field dependence parameter is lower than 10% and commonly mimics trends of κ. For three pumice samples from profile 4a (Figure 2b), only magnetic susceptibility was measured, which was in the low paramagnetic range and therefore excluded from any further measurements.

The κ(T) measurements typically revealed two to four different transition temperatures (T_T) present in all samples (Figure 2, right column). Low-temperature runs rarely show evidence for the Verwey transition (Figure 3), indicating a lack of stoichiometric magnetite. The lack of the Verwey transition in the few low-temperature κ(T) curves done in this study (Table S1 in Supporting Information S1) suggests more than 3.5 atomic% of Ti in the crystal lattice (Kosterov et al., 2009; Kozłowski et al., 1996). High-temperature susceptibility measurements yield T_T mostly between 0 and 200°C, 250–400°C, and >400°C, which indicate the presence of magnetic phases with various Ti concentrations (all κ(T) data sets are available in Data Sets S1–S4 in Supporting Information S1). According to formula 1 given in Lattard et al. (2006), we have calculated the content of ulvöspinel (X_{Usp}) that is changing in a wide range from X_{Usp} = 0.06–0.18 for T_T > 500°C through X_{Usp} = 0.44 for T_T ~ 300°C and X_{Usp} = 0.68–0.78 for T_T < 100°C. The thermomagnetic curves are generally reversible above 550°C and become quasi-reversible (Figures 3a, 3b and 3d) or nonreversible (Figures 3c, 3e and 3f) at lower temperatures. Transition temperatures are more or less comparable within the same eruption sequences (Figure 2, right column), displaying a characteristic κ(T) behavior for the different pyroclastic deposits (Figure 3). Transition temperatures indicated on cooling runs are typically lower or similar to those observed on heating curves (Figure 2, right column, Figure 3). In a few pumice sections (see, e.g., profile 2 in Figure 2a), cooling runs show higher T_T than the heating runs.

The magnetic minerals were further characterized by hysteresis parameters (Figure 4). All measured loops are a mixture of paramagnetic and ferromagnetic signals, but once the slope correction is done, a clear ferromagnetic component is obtained. Hysteresis loops display a wide range of shapes from very narrow through wasp-waisted and pot-bellied. When plotted on the Day diagram (Figure 4e), most of the samples are placed in the PSD (vortex) area. For most of the samples, hysteresis parameters show a strong variation except for pumice deposits, which show the highest H_{cr}/H_c ratios and the most congruent cluster (Figure 4e; squares). The data on a squareness-coercivity plot (Figure S1 in Supporting Information S1) show a linear trend, suggesting that all samples have similar magnetic minerals but varying grain sizes. Plotting the trends for low Ti-magnetite and TM60 (Wang & Van der Voo, 2004), our data plot between the trends, suggesting that the samples are likely oxidized. Moreover, there seems to be no apparent trend in the distribution of hysteresis parameters with depth (Table S2 in Supporting Information S1) except for coercivity (Hc), which is rather constant throughout all profiles (<20 mT) and reaches the lowest values for pumice sections (<5 mT; Table S2 in Supporting Information S1).

The isothermal remanence magnetization (IRM) acquisition curves were found to be similar for all pyroclastic deposits and reach saturation at fields below 250–300 mT, which suggests the dominance of low coercivity (titano-)magnetite minerals of pseudo-single-domain (PSD) grain size. The IRM modeling indicated at least three components in these samples (Figure 5 and Table S1 in Supporting Information S1). C1 is a soft component with $B_{1/2}$ ~30–70 mT and dispersion parameter (DP) 0.25–0.40 (log units) that is the major contributor to the total IRM (>40%); C2 is a relatively hard component with $B_{1/2}$ >200 mT, DP ranges between 0.10 and 0.30 and the contribution of this phase is usually not exceeding 15%. Component C3 is very soft with $B_{1/2}$ usually below 20 mT and DP in a range of 0.20–0.40. This component has various contributions depending on the type of pyroclastic deposits from less than 15% for most block-and-ash flows and up to 40% for pumice samples. Some samples also show a fourth component (C4) with coercivity either between 20 and 70 mT or over 100 mT and quite wide DP (0.20–0.40). The content of C4 is widely varying up to 40% (Figure 5g). Profile 4 shows a scatter of mean coercivity values (Figure 5). Component 1 is classified as low-Ti titanomagnetite (likely exsolved), C2

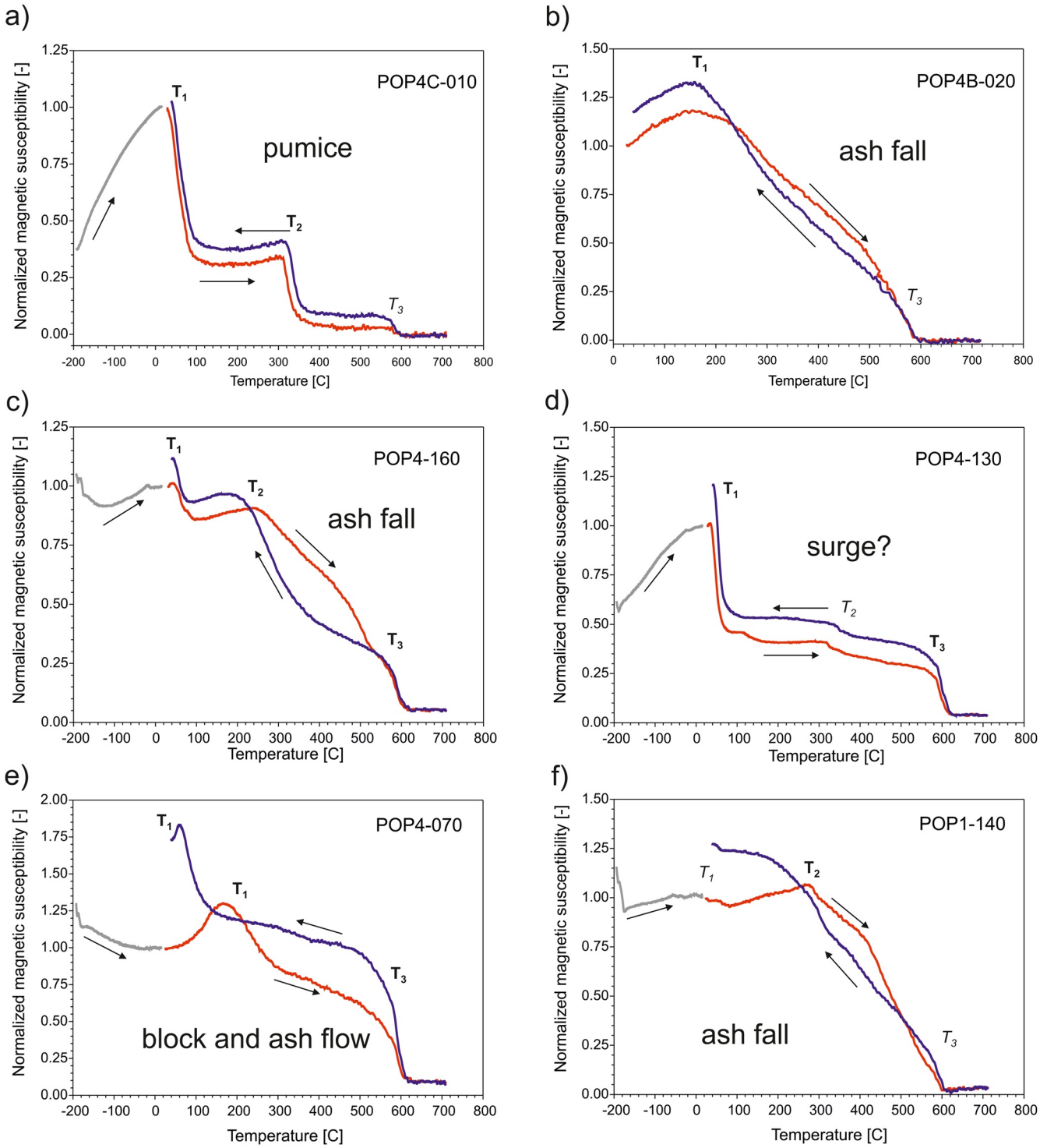

Figure 3. (a–f) Thermomagnetic curves κ(T) for representative samples normalized to κ at room temperature. Arrows indicate heating and cooling runs. The last three digits in the sample ID (e.g., POP4C-010) indicate the depth in cm shown in Figure 2. $T_{1,2,3}$ indicate transition temperatures of the dominant phase (bold) and minor (italic) phase.

is indicated as (ilmeno)hematite, C3 as high-Ti titanomagnetite (homogenous), and C4 as titanomagnetite or titanomaghemite with intermediate content of Ti of varying grain size. Whereas C2 cannot be seen directly on κ(T) curves, the remaining components can be separated and correlated with T_T (Figures 5a, 5c, 5e, 5h and 5j).

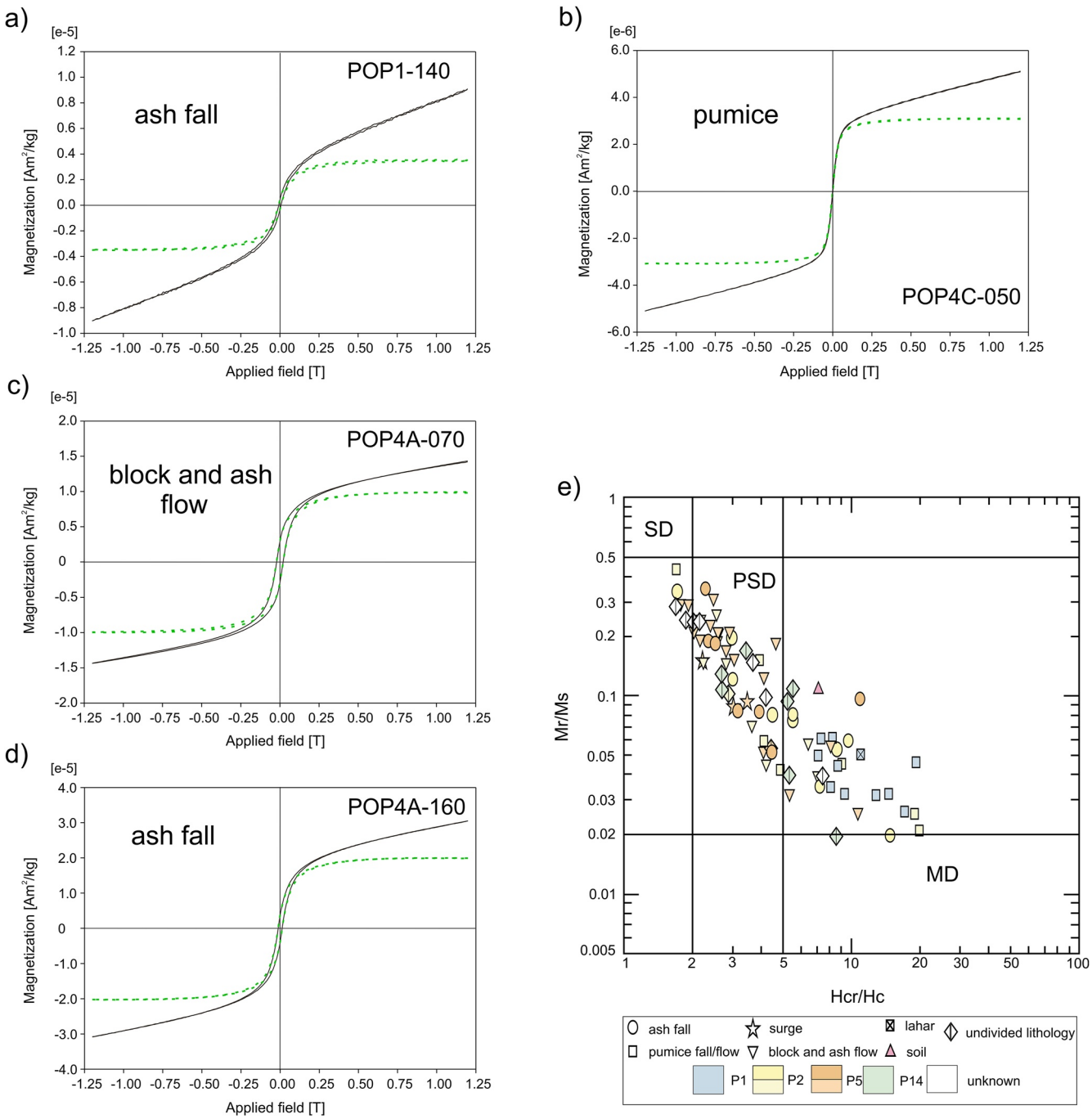

Figure 4. (a–d) Representative examples of room temperature hysteresis loops from the studied profiles; (e) M_{rs}/M_s versus H_{cr}/H_c for all profiles plotted on the Day diagram (Day et al., 1977). The solid line indicates the hysteresis loop before correction for paramagnetic minerals, and the dashed green line represents the corrected loop. The last three digits in the sample ID (e.g., POP4C-010) indicate the depth in cm shown in Figure 2.

It should be noted that component C1 dominating the IRM properties is often used for emplacement temperature determination of pyroclastic deposits (e.g., Lerner, Cronin, & Turner, 2019). However, this component is not always the major contributor to magnetic susceptibility.

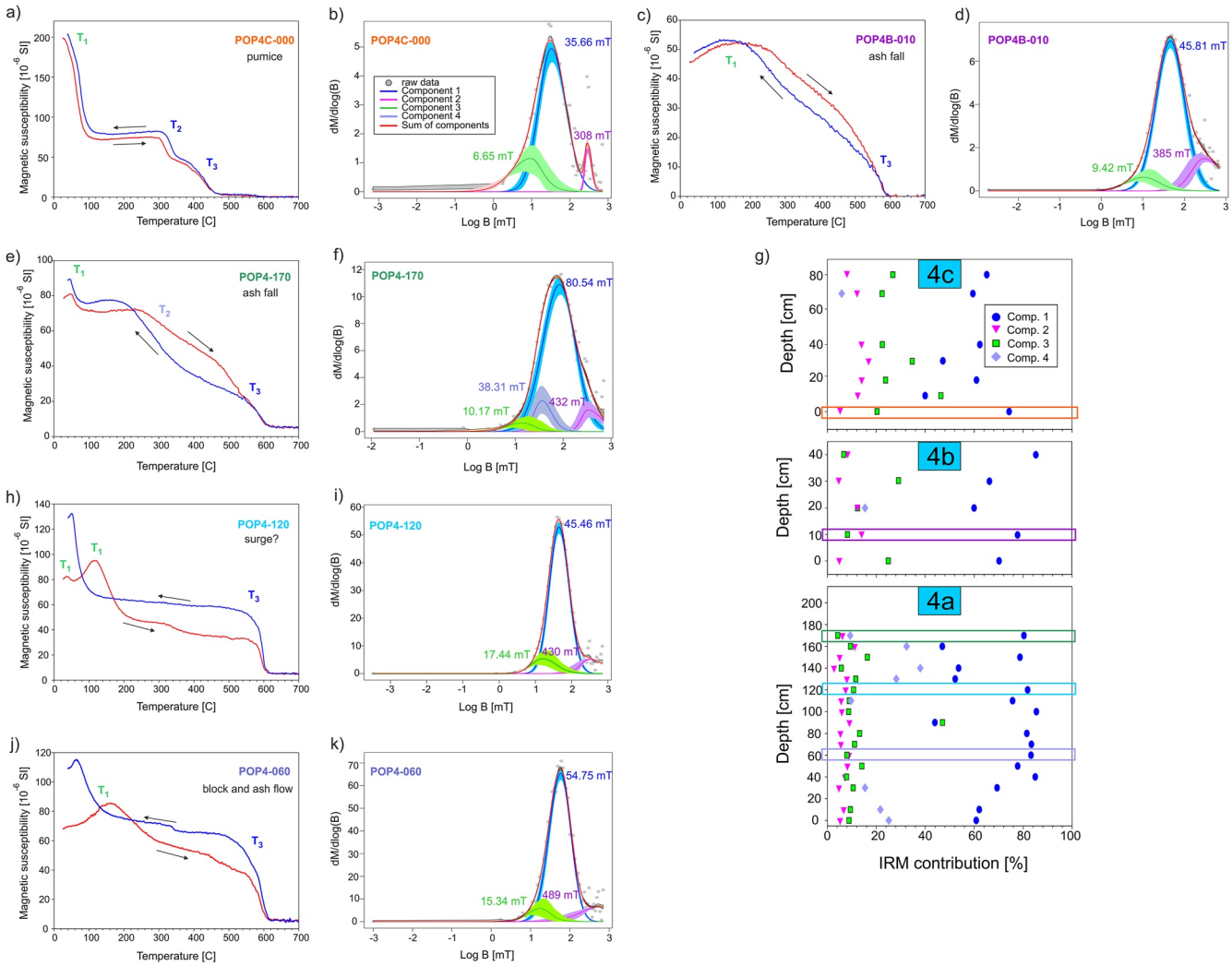

Figure 5. Examples of κ(T) curves (a, c, e, h, j) and corresponding IRM decomposition plots (b, d, f, i, k) for representative samples of different pyroclastic deposits from profile 4 using Max Unmix software (Maxbauer et al., 2016). The values of $B_{1/2}$ for each component are indicated on the plots. (g) Contribution of each component to total IRM. Color-coding was applied to correlate transition temperature with matching IRM components (e.g., comp. 1 corresponding to T_3 is given in blue). Please note that component 2 (pink/magenta) is not observed in κ(T) curves. The last three digits in the sample ID (e.g., POP4C-010) indicate the depth in cm shown in Figure 2. Arrows indicate heating and cooling runs. $T_{1,2,3}$ indicate transition temperatures of the dominant phase (bold) and minor (italic) phase.

4.2. Fe-Ti Oxide Mineral Assemblages

Reflected light and scanning electron microscopy revealed that, as expected, the pyroclastic deposits consist of a heterogeneous mixture of lithic clasts and glass fragments (Figure 6). The Fe-Ti oxides are generally xenomorphic to hypidiomorphic and show variation in grain size from <10 μm to approximately 100 μm. They belong to the titanomagnetite (tmt) and ilmenohematite (ilhm) solid solution series and show various stages of oxidation related to deuteric oxidation. Homogenous titanomagnetite and ilmenohematite grains (Figures 6a–6e) display a low degree of oxidation and thus can be assigned to the C1 and R1 oxidation states for titanomagnetite and ilmenite, respectively (Haggerty, 1976, 1991). These grains typically exhibit cracks, which may indicate fracturing during the dome collapse and eruption. Larger grains of Fe-Ti oxides are mostly intergrown with plagioclase and pyroxene phenocrysts, which also show cracks (Figures 6a and 6d). Smaller grains of homogenous titanomagnetite frequently show vermicular intergrowth with pyroxene (Figures 6b and 6c). This type was mainly observed in pumice samples and is indicative of the more evolved magma from the shallow magma reservoir (e.g., Mangler et al., 2020). Additionally, ilmenohematite with titanomagnetite lamellae of the composite type as well as of the sandwich type occurs, indicating a higher state of oxidation (C3-4, R2-3, Figures 6e and 6f). Although those grains seem to be homogenous under the reflected light, the application of ferrofluid revealed

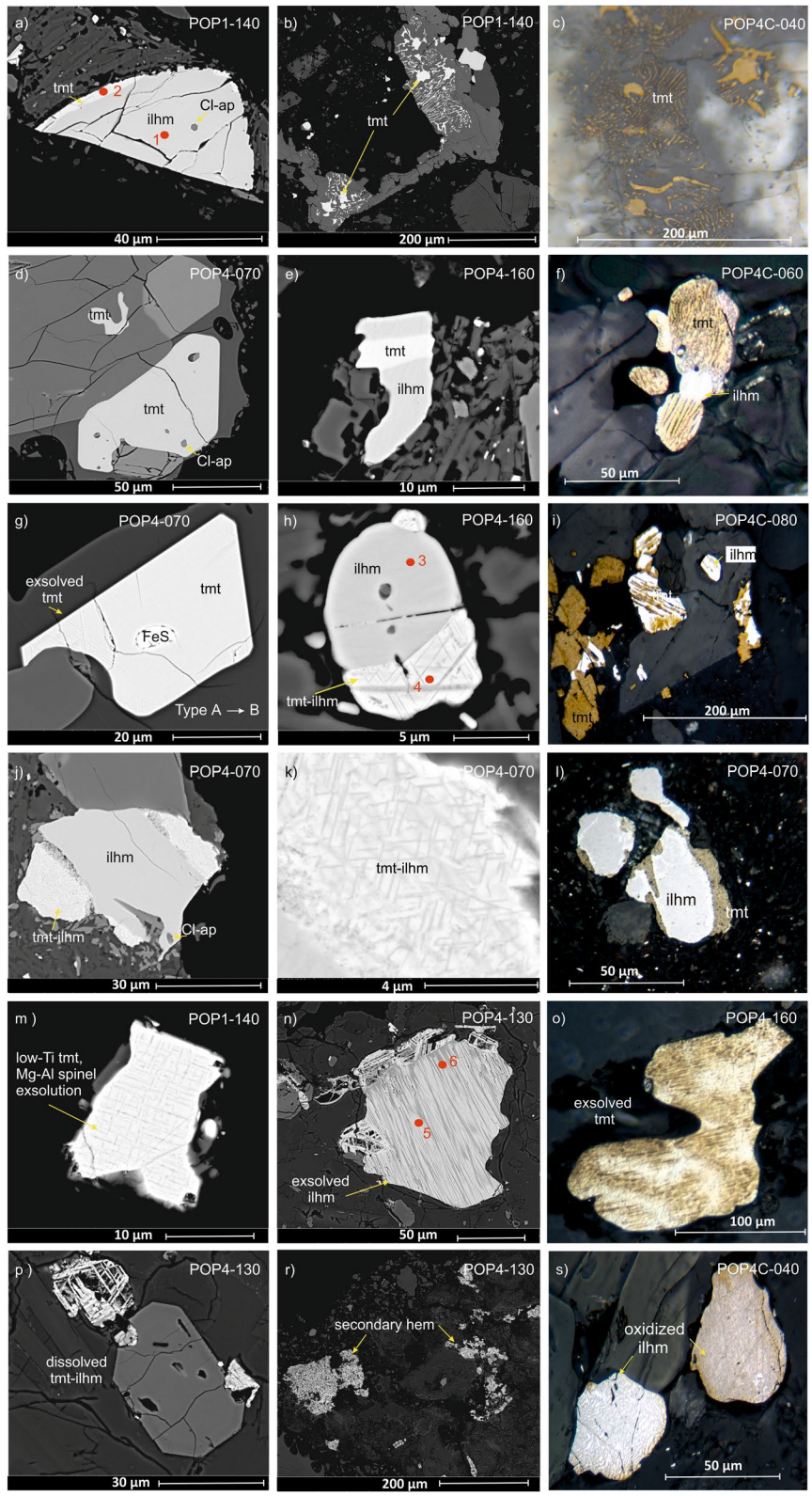

Figure 6. Scanning electron microscope (a, b, d, e, g, h, j, k, m, n, p, r) and reflected light (c, f, i, l, o, s) photographs of representative grains from different pyroclastic deposits reflecting different oxidation stages. Mainly homogenous grains of Fe-Ti oxides (a–f) were classified as type A, whereas exsolved (g–l) and oxidized grains (m–s) can be attributed to types B and C, respectively (according to the classification scheme of Saito et al. (2007)). For better distinction of the Fe-Ti-oxides, ferrofluid and oil immersion were used for reflected light microscopy. Abbreviations: ilhm—ilmenohematite, hem—hematite, tmt—titanomagnetite, and Cl-ap—chloroapatite. EDS spectra of red spots in (a), (h), and (n) are shown in Figure S2 in Supporting Information S1.

thin exsolution lamellae of titanomagnetite in ilmenohematite (Figure 6f). The homogeneity of these Fe-Ti oxide grains and low degrees of oxidation suggests that these minerals were formed in the inner part of the lava dome (type A according to Saito et al., 2007) and/or in the shallow magma chamber before an eruption. However, a great majority of the titanomagnetite grains also show exsolution-lamellae of ilmenite/ilmenohematite along {111} that are either thick (up to 30 μm, Figure 6i) or very thin (∼1 μm, Figures 6g, 6h, 6j and 6k) and can be assigned to the trellis type with oxidation level C2 or C3 (Haggerty, 1976, 1991). Iron sulfide (Figure 6g) or thin hematite exsolution (Figure 6l) is also present. Grains with lamellae exsolution are suggested to be the result of oxidation of homogenous titanomagnetite grains and can be classified as type B according to Saito et al. (2007). Figures 6m–6s show Fe-Ti oxide grains with dissolution features and pronounced exsolution indicating very high oxidation stages (type C, Saito et al., 2007). In these cases, titanomagnetite mostly shows oxidation in the form of thick trellis-type ilmenite lamellae and broad composite-type lamellae together with secondary hematite. Figure 6n even shows ilmenite-rutile (or pseudobrookite) exsolution lamellae. According to Haggerty (1991), these oxidation states correspond to stage C4/R4 or higher. EDS spectra indicate a large variation in Ti concentration with a minor contribution of Al as well as Mg and Cr (Figure S2 in Supporting Information S1).

5. Discussion

Our rock magnetic and magnetic mineralogy study of the Plinian eruptive sequences over the last 14,000 years from the Popocatépetl volcano has shown a complex ferrimagnetic Fe-Ti oxide mineral assemblage, especially for the P5, P2, and P1 with at least two, commonly three, or more different T_C (named as transition temperatures in Figures 2 and 3), indicating different titanomagnetite compositions. The T_C distribution (Figure 2) agrees well with IRM modeling (Table S1 in Supporting Information S1) and the microscopic observations, which reveal homogenous titanomagnetites with high or intermediate Ti content and exsolved titanomagnetite grains with compositions near the endmember magnetite (Figure 6 and Figure S2 in Supporting Information S1). The latter feature is typical for high-temperature oxidation of titanomagnetite in igneous rocks (Haggerty, 1976, 1991). According to Bowles et al. (2015), oxyexsolution of magnetic phases into low-Fe ilmenite and low-Ti magnetite and the relative reversibility of thermomagnetic curves (Figure 3) indicate deposition with little or no low-temperature post-emplacement alteration that can sometimes affect pyroclastic deposits (Lerner, Cronin, Turner, et al., 2019). Therefore, homogeneous titanomagnetite (type A) and exsolved titanomagnetite (type B−C) in different proportions are the most abundant ferromagnetic minerals in the PDCs.

The determined T_C from κ(T) curves show a good correlation with components obtained through IRM modeling from hysteresis data (Figure 5). Three main components are observed, which we interpret as high-coercivity Ti-poor (exsolved) titanomagnetite (C1), higher coercivity ilmenohematite (C2; the strongest oxidized Fe-Ti oxide), and low coercivity Ti-rich titanomagnetite (C3; homogeneous). In addition, some samples show a medium coercivity component (C4), most likely related to intermediate titanomagnetite/titanomaghemite, which, however, is not easy to distinguish from the exsolved Ti-poor titanomagnetite (Figure 5). In nearly all samples, component 1 clearly dominates the hysteresis properties and the remanent magnetization (Table S2 in Supporting Information S1). This high-coercivity phase with T_C close to 580°C is found and used in many paleomagnetic studies related to the determination of the emplacement temperature (e.g.Alva-Valdivia et al., 2019; Lerner, Cronin, & Turner, 2019; Lerner, Cronin, Turner, et al., 2019). Hysteresis parameters for most of our investigated pyroclastic deposit types indicate pseudo-single domain behavior with varying magnetization and coercivities (Figure 4 and Figure S1 in Supporting Information S1).

Jackson et al. (1998) demonstrated that the field dependence of magnetic susceptibility in titanomagnetite is dominantly controlled by the composition, and linear regression ($R^2 = 0.97$) exists between T_C and log χ_{Hd} (de Wall, 2000). We observed that a strong scattering of this relation (Figure S3 in Supporting Information S1) is typical for volcanic rocks with mixed homogeneous and exsolved titanomagnetite assemblages, which agrees with observations of Vahle and Kontny (2005). A combination of T_C determination and field dependence of magnetic susceptibility helps to qualitatively distinguish the amount of the different contributions, although other factors besides composition, such as the measurement temperature, grain size, and anisotropy (Vahle & Kontny, 2005), might contribute to a scattering of the T_c−χ_{Hd} relation. Titanomagnetite with a $T_C < 100$°C, observed in the sequences with high χ_{Hd} (Figure 2), shows around room temperature a peak-type behavior (e.g., Lattard et al., 2006). Field dependence of this peak is significant as shown in Vahle and Kontny (2005; see their Figure 4) and therefore might indicate an erroneously high concentration of the homogeneous Ti-rich

titanomagnetite. Therefore, χ_{Hd} can give a first trend, for example, in pumice deposits but the component analysis obtained through IRM modeling is much more reliable. Titanomaghemite does not show a field dependence in magnetic susceptibility at all (e.g., Vahle & Kontny, 2005). We relate the nonreversible intermediate transition temperatures in the range of 300–500°C to titanomaghemite (Figures 2, 3b and 7, yellow ovals) and assume that they do not contribute much to χ_{Hd}.

A clear dominance of high T_C is observed in the P14 sequence and in profile 3a of the P5 sequence, suggesting that the volcanic material in the block-and-ash flow originates from the collapse of an endogenous lava dome (Figure 7). In profile 4a of the same P5 sequence, we also observe lower T_C in accordance with homogeneous titanomagnetite, indicating lateral changes in the P5 block-and-ash flow (Figures 2 and 7). This block-and-ash flow (see profile 4a in Figures 2b and 7) shows significant and systematic nonreversibility of the T_C for the homogeneous Ti-rich titanomagnetite (Figures 3e and 6d) with ΔT_C ($T_{C\,heating} - T_{C\,cooling}$) up to 130°. The Ti-poor oxy-exsolved titanomagnetite grains are unaffected and show reversible T_Cs in the heating and cooling runs. Interestingly, this block-and-ash flow deposit (Figure 2, profile 4a) shows a decrease in magnetic susceptibility and field dependence of magnetic susceptibility and an increase in ΔT_C of the Ti-rich titanomagnetite from the bottom to the central part. This homogeneous titanomagnetite shows a different behavior than those of most other sequences because the irreversibility of T_C is the largest (compare T_1 in Figures 3c and 3e).

Curie temperature irreversibility can be either due to vacancy-enhanced nanoscale chemical clustering (Bowles et al., 2019) or maghemitization (e.g., Lied et al., 2020; Oliva-Urcia et al., 2011). Their distinction is difficult because cation vacancies (□) follow independent of process the paired substitution $3Fe^{2+} = 2Fe^{3+} + □$ (Jackson & Bowles, 2018). Cation vacancies can be due to oxygen fugacity at titanomagnetite crystallization temperatures (e.g., Lattard et al., 2006) or due to low-temperature oxidation. This issue could be solved by the chemical analysis, high-resolution transmission electron microscopy, or X-ray magnetic circular dichroism (Bowles et al., 2019). One approach is also the use of progressive heating-cooling cycling experiments (Jackson & Bowles, 2018, and references therein), which shows reversible changes in ΔT_C, indicating that no bulk chemical alteration

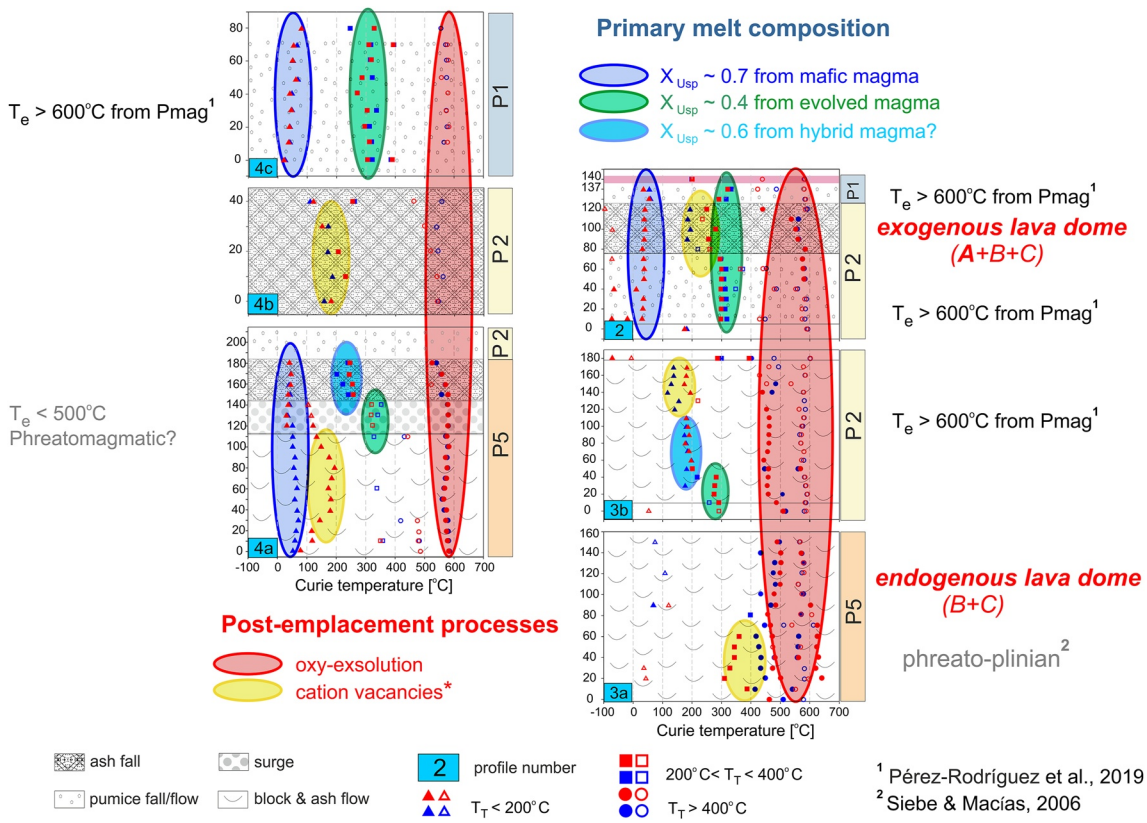

Figure 7. Schematic compilation of T_C and correlation with primary melt composition and post-emplacement processes for pyroclastic density deposits of the Popocatépetl volcano. Abbreviation: Te—emplacement temperature; * cation vacancies from crystallization of the melt or due to maghemitization.

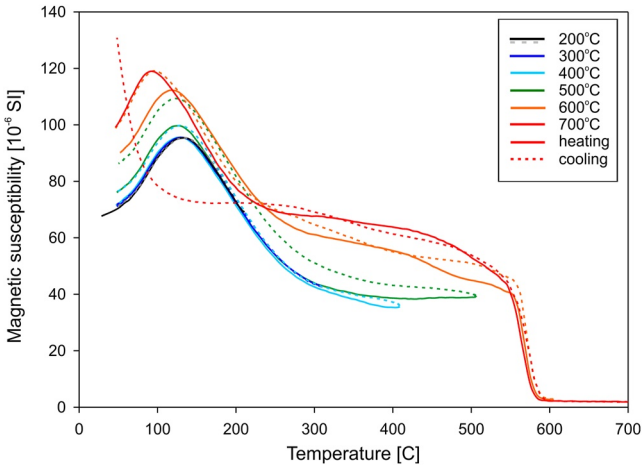

Figure 8. Repeated progressive heating-cooling cycles of sample POP4-80 at heating/cooling rates of 10 K/min in 100°C steps up to 700°C (measured in argon). Solid and dashed lines indicate heating and cooling curves, respectively.

is involved for vacancy-enhanced nanoscale chemical clustering below the titanomagnetite binary solvus for compositions between $0.25 < x < 0.6$ (Bowles et al., 2019).

For sample POP4-80, we performed heating-cooling experiments in an inert Ar atmosphere at heating/cooling rates of 10 K/min in 100°C steps up to 700°C, which is the temperature that is generally used for κ(T) measurements. We observed that up to 500°C, which is the limit of the titanomagnetite binary solvus for intermediate compositions, the heating, and following cooling curves are all reversible. But at 600 and 700°C, T_C decreases progressively (Figure 8), likely indicating that the closure temperature is overstepped. We interpret this behavior in the way that the natural sample was rapidly quenched from a temperature >700°C. In this sample, we also observe a distinct increase in magnetic susceptibility in the temperature range between 580°C and the peak-type behavior below approximately 250°C in the cooling curve for experiments ≥500°C. We suggest that this feature is related to a new formation of tiny magnetite grains from hematite (observed under reflected light microscopy) during the measurement in an Ar atmosphere and is not related to an exsolution texture in titanomagnetite as the titanomagnetite remains homogeneous after the experiment. These data clearly confirm that ΔT_C is sensitive to the thermal history of titanomagnetite in PDCs.

The basal pyroclastic surge deposit of the P5 sequence in profile 4a is reported to be formed from an initially phreatomagmatic explosion with a short but intense activity (Arana-Salinas et al., 2010; Siebe et al., 1996), which is in line with rapid cooling of the material. Generally, Plinian volcanic eruptions are reported to be emplaced at higher emplacement temperatures than phreatomagmatic eruptions (e.g., Fontana et al., 2011; Lesti et al., 2011; Porreca et al., 2008), but if the pyroclastic material gets into contact with glacial ice or water-filled gullies, the cooling rate can be significantly changed. Similar nonreversible behavior of T_C was previously not only observed in pyroclastic deposits from Mount St. Helens, USA (Bowles et al., 2013) but also in the Mýtina Maar, Czech Republic (Lied et al., 2020), where phreatic phases were also reported as a (pre-) eruptive stage (Cashman & Hoblitt, 2004; Mrlina et al., 2007). In all these deposits, a significant amount of juvenile clasts is observed, suggesting that not only eruption style but also the contribution of different composed juvenile material might play a role in the nonreversibility of T_C.

Interestingly, we observed lateral and vertical (within and across different lithological deposits) changes in the magnetic mineralogy (Figures 2 and 7), suggesting spatially and temporally different emplacement conditions during the same and following events. In the block-and-ash flow of the P5 sequence seen in profile 3a, we recognized a higher amount of exsolved titanomagnetite compared to the block-and-ash flow deposit of the younger P2 sequence in profile 3b, which is characterized by a significant amount of homogeneous titanomagnetite (Figure 7). This observation suggests more endogenous (P5) or exogenous (P2) lava dome material that collapsed during the PDC generation. While in the lower P5 sequence, T_C between approximately 490°C and 580°C indicates an ulvöspinel component (X_{usp}) of 0.20 to pure magnetite, the higher (and younger) P2 sequence contains a more distinct contribution of homogeneous titanomagnetite with T_C of approximately 170°C (X_{usp} of 0.61) and 300°C (X_{usp} of 0.44; according to formula 1 given in Lattard et al., 2006). We relate these different compositions of the homogeneous titanomagnetite to the mafic and more evolved magma reservoir, respectively. Moreover, the presence of Cr in the Ti-Fe oxides observed in our study is in line with previous reports on magma mixing (Sosa-Ceballos et al., 2014). Field-dependent magnetic susceptibility (χ_{Hd}) in the block-and-ash flow of sequences P5 and P2 is similar (4%–8%) and does not clearly indicate a higher concentration of homogeneous titanomagnetite (Figure 2).

A different pattern is observed in the pumice fall and flow of the P2 sequence (profile 2), in which high χ_{Hd} values between 10% and 20% indicate a significant contribution of homogeneous titanomagnetite (Figure 2b). This is also the case in the pumice fall and flow of the P1 sequence (profile 4c), in which high χ_{Hd} values of around 20% occur. In these samples, even two or three Ti-rich titanomagnetite compositions dominate, one with a $T_C < 100$°C and others with T_Cs between 200 and 300°C, in agreement with the high χ_{Hd}. These T_C indicate X_{usp} between 0.76 and 0.44 (Lattard et al., 2006) and likely indicate different Ti/(Ti + Fe) ratios or oxygen fugacity

of the melt (Figure 7), which is in line with petrologic studies of Mangler et al. (2020) suggesting at least two long-lived, interconnected magmatic environments as well as hybrid conditions between these two. In sequences with high χ_{Hd} values, homogeneous titanomagnetite has a significant contribution to the remanent magnetization (see Table S1 in Supporting Information S1) although the magnetic susceptibility (induced magnetization) is low (Figure 2 and Table S2 in Supporting Information S1). Within the P2 sequence, we clearly observe a change from evolved to possibly hybrid magma environments in the basal deposits with an additional mafic magma component in the upper sequences (Figure 7). Intermediate titanomagnetite compositions with slightly irreversible T_C (yellow in Figure 7) are interpreted to reflect maghemitization although a distinction from vacancy-enhanced nanoscale chemical clustering is difficult based on κ(T) curves only. This type was not observed in pumice from the P1 sequence. Pérez-Rodríguez et al. (2019) argued from paleomagnetic and rock magnetic data that the emplacement temperatures of the P1 and P2 sequences from the Popocatépetl volcano were hot, above the T_C of magnetite (580°C), because the original magnetization of the clasts is reset. This means that all clasts carry a thermoremanent magnetization throughout the whole blocking temperature spectrum aligned with the field at the time of cooling. In our study, most Ti-poor, intermediate, and Ti-rich titanomagnetite from the P1 sequence show reversible T_C (Figures 2, 3a, and 7), suggesting cooling along an equilibrium path (see Figure 6 in Jackson & Bowles, 2014), which agrees well with the paleomagnetic investigations (Pérez-Rodríguez et al., 2019).

6. Conclusions

We performed bulk, field, and temperature-dependent magnetic susceptibility; determined the hysteresis properties; and combined these data with microscopic observations from different pyroclastic eruptive sequences of the Popocatépetl volcano in order to obtain information on the primary titanomagnetite composition and the volcanic material history (Figure 7). Our study showed that exsolved titanomagnetite with T_Cs between 500° and 580°C is the most important carrier of the magnetization, which is mainly used in the paleomagnetic studies for emplacement temperature determination. We have shown that magnetic susceptibility, microscopy, and T_C help to unravel distinct magnetic features that are related to the emplacement processes during the pyroclastic deposition and may aid as a complementary approach to the paleomagnetic directional analysis for emplacement temperatures. The most characteristic magnetic features in our study are reversible T_Cs that are either related to homogeneous or exsolved titanomagnetites in line with a high crystallization or emplacement temperature that allowed a cooling along the equilibrium path. The exsolved titanomagnetite can either come from an endogenous dome collapse or a hot emplacement and subaerial oxy-exsolution after deposition. We recognized an increase of homogeneous titanomagnetite (component C3 from IRM modeling) from older P5 to younger P1 sequences with reversible T_Cs in the lower part and little nonreversibility of the intermediate titanomagnetite in the upper part of the sequence, which might indicate subtle maghemitization. Pumice deposits can be characterized by low values of magnetic susceptibility, high field dependence, and reversible T_C correlated with a high concentration of Ti-rich titanomagnetite. The highest scattering of magnetic parameters is observed in block-and-ash-flow deposits of P5 sequence that also exhibit high ΔT_C, interpreted to indicate rapid quenching, presumably because of a phreatomagmatic explosion (Arana-Salinas et al., 2010). Therefore, we were able to show the potential of the combination of different susceptibility measurements along with hysteresis measurements for the distinction of different eruptive sequences and propose this approach as an alternative or addition to study emplacement processes in pyroclastic deposits. Titanomagnetite composition crystallized from melt and post-crystallization processes like high-temperature oxidation, rapid cooling, or maghemitization can be discriminated.

Conflict of Interest

The authors declare no conflicts of interest relevant to this study.

Data Availability Statement

Data to support this article are deposited in Mendeley as Dudzisz, K. et al. (2022), https://doi.org/10.17632/9g2tszftvr.2 and also uploaded to the Magnetic Information Consortium rock magnetic portal (https://earthref.org/MagIC/19591/206809c5-acfc-41e3-b4cb-411630a7025e) at CC-BY 4.0.

Acknowledgments
LA thanks DGAPA-UNAM research project IN101521 for financial support. We would like to thank Volker Zibath for his support at the SEM. Thanks to Ana Lillian Martin del Pozzo and Alejandro Rodríguez-Trejo for guiding and support during fieldwork, Antonio González-Rangel for performing the hysteresis experiments, as well as Christoph Meister, Alexander Spitzner, and Kai Pascal Hermann for measuring κ(T) curves. The reviews of Greig Paterson, Stefanie Brachfeld, Michael Ort, and an anonymous reviewer, as well as editor Joshua Feinberg, helped us to clarify this paper. Open Access funding enabled and organized by Projekt DEAL.

References

Alva-Valdivia, L. M., Rodríguez-Trejo, A., Vidal-Solano, J. R., Paz-Moreno, F., & Agarwal, A. (2019). Emplacement temperature resolution and age determination of Cerro Colorado tuff ring by TRM analysis, El Pinacate Volcanic field, Sonora. Mexico. *Journal of Volcanology and Geothermal Research*, *369*, 145–154. https://doi.org/10.1016/j.jvolgeores.2018.11.012

Arana-Salinas, L., Siebe, C., & Macías, J. L. (2010). Dynamics of the ca. 4965 14C yr BP ''Ochre Pumice'' plinian eruption of Popocatépetl Volcano, México. *Journal of Volcanology and Geothermal Research*, *192*(3–4), 212–231. https://doi.org/10.1016/j.jvolgeores.2010.02.022

Banks, N. G., & Hoblitt, R. P. (1996). Direct temperature measurements of deposits, Mount St. Helens, Washington, 1980-1981. In *USGS professional Paper 1387* (p. 83). U.S. Government Printing Office.

Bowles, J. A., Gee, J. S., Jackson, M., & Avery, M. S. (2015). Geomagnetic paleointensity in historical pyroclastic density currents: Testing the effects of emplacement temperature and postemplacement alteration. *Geochemistry, Geophysics, Geosystems*, *16*(10), 3607–3625. https://doi.org/10.1002/2015GC005910

Bowles, J. A., Gerzich, D. M., & Jackson, M. J. (2018). Assessing new and old methods in paleomagnetic paleothermometry: A test case at Mt. St. Helens, USA. *Geochemistry, Geophysics, Geosystems*, *19*(6), 1714–1730. https://doi.org/10.1029/2018GC007435

Bowles, J. A., Jackson, M. J., Berquó, T. S., Sølheid, P. A., & Gee, J. S. (2013). Inferred time- and temperature-dependent cation ordering in natural titanomagnetites. *Nature Communications*, *4*(1), 1916. https://doi.org/10.1038/ncomms2938

Bowles, J. A., Lappe, S.-C. L. L., Jackson, M. J., Arenholz, E., & van der Laan, G. (2019). Curie temperature enhancement and cation ordering in titanomagnetites: Evidence from magnetic properties, XMCD, and Mössbauer spectroscopy. *Geochemistry, Geophysics, Geosystems*, *20*, 2272–2289. https://doi.org/10.1029/2019GC008217

Brachfeld, S. A., & Hammer, J. (2006). Rock-magnetic and remanence properties of synthetic Fe-rich basalts: Implications for Mars crustal anomalies. *Earth and Planetary Science Letters*, *248*(3–4), 599–617. https://doi.org/10.1016/j.epsl.2006.04.015

Cashman, K. V., & Hoblitt, R. P. (2004). Magmatic precursors to the 18 May 1980 eruption of Mount St. Helens, USA. *Geology*, *32*(2), 141–144. https://doi.org/10.1130/g20078.1

Christiansen, R. L., & Peterson, D. W. (1981). Chronology of the 1980 eruptive activity. In P. W. Lipman & D. R. Mullineaux (Eds.), *The 1980 eruptions of Mount St. Helens, Washington* (pp. 17–30). U.S. Department of the Interior, U.S. Geological Survey.

Cole, P. D., Neri, A., & Baxter, P. J. (2015). Chapter 54-hazards from pyroclastic density currents. In H. Sigurdsson (Ed.), *The encyclopedia of volcanoes* (2nd ed., pp. 943–956). Academic Press.

Day, R., Fuller, M., & Schmidt, V. A. (1977). Hysteresis properties of titanomagnetites: Grain size and compositional dependence. *Physics of the Earth and Planetary Interiors*, *13*(4), 260–266. https://doi.org/10.1016/0031-9201(77)90108-X

de Wall, H. (2000). The field dependence of AC-susceptibility in titanomagnetites: Implications for the anisotropy of magnetic susceptibility. *Geophysical Research Letters*, *27*, 2413–2416.

Denniss, A. M., Carlton, R. W. T., Harris, A. J. L., Rothery, D. A., & Francis, P. W. (1998). Satellite observations of the April 1993 eruption of Láscar volcano. *International Journal of Remote Sensing*, *19*(5), 801–821. https://doi.org/10.1080/014311698215739

Dunlop, D. J., & Özdemir, Ö. (1997). *Rock magnetism: Fundamentals and frontiers*. Cambridge University Press.

Fontana, G., Niocaill, C. M., Brown, R. J., Sparks, R. S. J., & Field, M. (2011). Emplacement temperatures of pyroclastic and volcaniclastic deposits in kimberlite pipes in southern Africa. *Bulletin of Volcanology*, *73*(8), 1063–1083. https://doi.org/10.1007/s00445-011-0493-9

Gómez-Vázquez, A., De la Cruz-Reyna, S., & Mendoza-Rosas, A. T. (2016). The ongoing dome emplacement and destruction cyclic process at Popocatépetl volcano, Central México. *Bulletin of Volcanology*. *78*(9), 78–58. https://doi.org/10.1007/s00445-016-1054-z

Haggerty, S. E. (1976). Oxidation of opaque mineral oxides in basalts. In D. Rumble (Ed.), *Oxide minerals short course notes* (Vol. 3, pp. 1–100). Mineralogical Society of America.

Haggerty, S. E. (1991). Oxide textures – A Mini-atlas. *Reviews in Mineralogy and Geochemistry*, *25*, 129–219.

Harrison, R. J., & Putnis, A. (1999). Determination of the mechanism of cation ordering in magnesioferrite ($MgFe_2O_4$) from the time- and temperature-dependence of magnetic susceptibility. *Physics and Chemistry of Minerals*, *26*(4), 322–332. https://doi.org/10.1007/s002690050192

Jackson, M., Moskowitz, B., Rosenbaum, J., & Kissel, C. (1998). Field-dependence of AC susceptibility in titanomagnetites. *Earth and Planetary Science Letters*, *157*(3–4), 129–139. https://doi.org/10.1016/S0012-821X(98)00032-6

Jackson, M. J., & Bowles, J. A. (2014). Curie temperatures of titanomagnetite in ignimbrites: Effects of emplacement temperatures, cooling rates, exsolution, and cation ordering. *Geochemistry, Geophysics, Geosystems*, *15*(11), 4343–4368. https://doi.org/10.1002/2014GC005527

Jackson, M. J., & Bowles, J. A. (2018). Malleable Curie temperatures of natural titanomagnetites: Occurrences, modes, and mechanisms. *Journal of Geophysical Research: Solid Earth*, *123*(2), 921–920. https://doi.org/10.1002/2017JB015193

Kosterov, A., Conte, G., Goguitchaichvili, A., & Urrutia-Fucugauchi, J. (2009). Low-temperature magnetic properties of andesitic rocks from Popocatepetl stratovolcano, Mexico. *Earth Planets and Space*, *61*(1), 133–142. https://doi.org/10.1186/bf03352893

Kozłowski, A., Kąkol, Z., Kim, D., Zaleski, R., & Honig, J. M. (1996). Heat capacity of Fe3−αMαO4 (M = Zn, Ti, $0 \leq \alpha \leq 0.04$). *Physical Review B*, *54*(17), 12093–12098. https://doi.org/10.1103/physrevb.54.12093

Lattard, D., Engelmann, R., Kontny, A., & Sauerzapf, U. (2006). Curie temperatures of synthetic titanomagnetites in the Fe-Ti-O system: Effects of composition, crystal chemistry, and thermomagnetic methods. *Journal of Geophysical Research*, *111*(B12), B12S28. https://doi.org/10.1029/2006JB004591

Lerner, G. A., Cronin, S. J., & Turner, G. M. (2019). Evaluating emplacement temperature of a 1000-year sequence of mass flows using paleomagnetism of their deposits at Mt. Taranaki, New Zealand. *Volcanica*, *2*(1), 11–24. https://doi.org/10.30909/vol.02.01.1124

Lerner, G. A., Cronin, S. J., Turner, G. M., & Piispa, E. J. (2019). Recognizing long-runout pyroclastic flow deposits using paleomagnetism of ash. *GSA Bulletin*, *131*(11–12), 1783–1793. https://doi.org/10.1130/B35029.1

Lerner, G. A., Jenkins, S. F., Charbonnier, S. J., Komorowski, J.-C., & Baxter, P. J. (2022). The hazards of unconfined pyroclastic density currents: A new synthesis and classification according to their deposits, dynamics, and thermal and impact characteristics. *Journal of Volcanology and Geothermal Research*, *421*, 107429. https://doi.org/10.1016/j.jvolgeores.2021.107429

Lesti, C., Porreca, M., Giordano, G., Mattei, M., Cas, R. A., Wright, H. M., et al. (2011). High-temperature emplacement of the Cerro Galan and Toconquis group ignimbrites (Puna plateau, NW Argentina) determined by TRM analyses. *Bulletin of Volcanology*, *73*(10), 1535–1565. https://doi.org/10.1007/s00445-011-0536-2

Lied, P., Kontny, A., Nowaczyk, N., Mrlina, J., & Kämpf, H. (2020). Cooling rates of pyroclastic deposits inferred from mineral magnetic investigations: A case study from the pleistocene Mýtina maar (Czech Republic). *International Journal of Earth Sciences*, *109*(5), 1707–1725. https://doi.org/10.1007/s00531-020-01865-1

Love, S. P., Goff, F., Counce, D., Siebe, C., & Delgado, H. (1998). Passive infrared spectroscopy of the eruption plume at Popocatépetl volcano, México. *Nature*, *396*(6711), 563–567. https://doi.org/10.1038/25109

Lube, G., Breard, E. C. P., Esposti-Ongaro, T., Dufek, J., & Brand, B. (2020). Multiphase flow behavior and hazard prediction of pyroclastic density currents. *Nature Reviews Earth & Environment*, *1*(7), 348–365. https://doi.org/10.1038/s43017-020-0064-8

Macías, J. L., Arce, J. L., García-Tenorio, F., Sosa-Ceballos, G., & Gardner, J. E. (2020). Source and behavior of pyroclastic density currents generated by Vulcanian-style explosions of Popocatépetl Volcano (Mexico) on 22 January 2001. *Journal of Volcanology and Geothermal Research*, *406*, 107071. https://doi.org/10.1016/j.jvolgeores.2020.107071

Mangler, M. F., Petrone, C. M., Hill, S., Delgado-Granados, H., & Prytulak, J. (2020). A pyroxenic view on magma hybridization and crystallization at Popocatépetl Volcano, Mexico. *Frontiers of Earth Science*, *8*, 362. https://doi.org/10.3389/feart.2020.00362

Mangler, M. F., Petrone, C. M., & Prytulak, J. (2022). Magma recharge patterns control eruption styles and magnitudes at Popocatépetl Volcano (Mexico). *Geology*, *50*(3), 366–370. https://doi.org/10.1130/G49365.1

Mangler, M. F., Prytulak, J., Gisbert, G., Delgado-Granados, H., & Petrone, C. M. (2019). Interplinian effusive activity at popocatepetl Volcano, Mexico: New insights into evolution and dynamics of the plumbing system. *Volcanica*, *2*(1), 45–72. https://doi.org/10.30909/vol.02.01.4572

Mastrolorenzo, G., Petrone, P. P., Pagano, M., Incoronato, A., Baxter, P. J., Canzanella, A., & Fattore, L. (2001). Herculaneum victims of vesuvius in AD 79. *Nature*, *410*(6830), 769–770. https://doi.org/10.1038/35071167

Maxbauer, D. P., Feinberg, J. M., & Fox, D. L. (2016). MAX UnMix: A web application for unmixing magnetic coercivity distributions. *Computers & Geosciences*, *95*, 140–145. https://doi.org/10.1016/j.cageo.2016.07.009

Mollo, S., Putirka, K., Iezzi, G., & Scarlato, P. (2013). The control of cooling rate on titanomagnetite composition: Implications for a geospeedometry model applicable to alkaline rocks from Mt. Etna volcano. *Contributions to Mineralogy and Petrology*, *165*(3), 457–475. https://doi.org/10.1007/s00410-012-0817-6

Mrlina, J., Kämpf, H., Geissler, W., & Van den Bogaard, P. (2007). Assumed quaternary maar structure at the Czech/German border between Mytina and Neualbenreuth (western Eger rift, Central Europe): Geophysical, petrochemical and geochronological indications. *Zeitschrift für Geologische Wissenschaften*, *35*, 213–230.

Oliva-Urcia, B., Kontny, A., Vahle, C., & Schleicher, A. M. (2011). Modification of the magnetic mineralogy in basalts due to fluid-rock interactions in a high-temperature geothermal system (Krafla, Iceland). *Geophysical Journal International*, *186*(1), 155–174. https://doi.org/10.1111/j.1365-246X.2011.05029.x

Paterson, G. A., Roberts, A. P., Mac Niocaill, C., Muxworthy, A. R., Gurioli, L., Viramonté, J. G., et al. (2010). Paleomagnetic determination of emplacement temperatures of pyroclastic deposits: An under-utilized tool. *Bulletin of Volcanology*, *72*(3), 309–330. https://doi.org/10.1007/s00445-009-0324-4

Pensa, A., Capra, L., & Giordano, G. (2019). Ash clouds temperature estimation. Implication on dilute and concentrated PDCs coupling and topography confinement. *Scientific Reports*, *9*(1), 5657. https://doi.org/10.1038/s41598-019-42035-x

Pensa, A., Porecca, M., Corrado, S., Giordano, G., & Cas, R. (2015). Calibrating the pTRM and charcoal reflectance (Ro%) methods to determine the emplacement temperature of ignimbrites: Fogo A sequence, São Miguel, Azores, Portugal, as a case study. *Bulletin of Volcanology*, *77*(3), 1–19. https://doi.org/10.1007/s00445-015-0904-4

Pérez-Rodríguez, N., Morales, J., Goguitchaichvili, A., & García-Tenorio, F. (2019). A comprehensive paleomagnetic study from the last plinian eruptions of popocatepetl volcano: Absolute chronology of lavas and estimation of emplacement temperatures of PDCs. *Earth Planets and Space*, *71*(1), 80. https://doi.org/10.1186/s40623-019-1059-x

Porreca, M., Mattei, M., Mac Niocaill, C., Giordano, G., McClelland, E., & Funiciello, R. (2008). Paleomagnetic evidence for low-temperature emplacement of the phreatomagmatic Peperino Albano ignimbrite (Colli Albani volcano, Central Italy). *Bulletin of Volcanology*, *70*(7), 877–893. https://doi.org/10.1007/s00445-007-0176-8

Ramírez-Uribe, J., Siebe, C., Oryaëlle Chevrel, M., Ferres, D., & Salinas, S. (2022). The late Holocene Nealtican lava-flow field, Popocatépetl volcano, central Mexico: Emplacement dynamics and future hazards. *Bulletin of the Geological Society of America*. https://doi.org/10.1130/B36173.1

Saito, T., Ishikawa, N., & Kamata, H. (2003). Identification of magnetic minerals carrying NRM in pyroclastic-flow deposits. *Journal of Volcanology and Geothermal Research*, *126*(1–2), 127–142. https://doi.org/10.1016/s0377-0273(03)00132-x

Saito, T., Ishikawa, N., & Kamata, H. (2004). Iron-titanium oxide minerals in block-and-ash-flow deposits: Implications for lava dome oxidation processes. *Journal of Volcanology and Geothermal Research*, *138*(3–4), 283–294. https://doi.org/10.1016/j.jvolgeores.2004.07.006

Saito, T., Ishikawa, N., & Kamata, H. (2007). Magnetic petrology of the 1991–1995 dacite lava of Unzen volcano, Japan: Degree of oxidation and implications for the growth of lava domes. *Journal of Volcanology and Geothermal Research*, *164*(4), 268–283. https://doi.org/10.1016/j.jvolgeores.2007.05.015

Sawada, Y., Sampei, Y., Hyodo, M., Yagami, T., & Fukue, M. (2000). Estimation of emplacement temperatures of pyroclastic flows using H/C ratios of carbonized wood. *Journal of Volcanology and Geothermal Research*, *104*(1–4), 1–20. https://doi.org/10.1016/s0377-0273(00)00196-7

Siebe, C., Abrams, M., Macías, J. L., & Obenholzner, J. (1996). Repeated volcanic disasters in Prehispanic time at Popocatépetl, Central Mexico: Past key to the future? *Geology*, *24*(5), 399–402. https://doi.org/10.1130/0091-7613(1996)024<0399:rvdipt>2.3.co;2

Siebe, C., & Macías, J. L. (2006). Volcanic hazards in the Mexico city metropolitan area from eruptions at Popocatépetl, Nevado de Toluca, and Jocotitlán stratovolcanoes and monogenetic scoria cones in the Sierra Chichinautzin volcanic field. In C. Siebe, J. L. Macías, & G. Aguirre (Eds.), *Neogene–quaternary continental margin volcanism. A perspective from Mexico* (Vol. 402, pp. 253–329). Geological Society of America, Special Publication.

Siebe, C., Salinas, S., Arana-Salinas, L., Macías, J. L., Gardner, J., & Bonasia, R. (2017). The ∼23, 500 y 14 C BP White Pumice Plinian eruption and associated debris avalanche and Tochimilco lava flow of Popocatépetl volcano, México. *Journal of Volcanology and Geothermal Research*, *333–334*, 66–95. https://doi.org/10.1016/j.jvolgeores.2017.01.011

Sosa-Ceballos, G., Gardner, J. E., & Lassiter, J. C. (2014). Intermittent mixing processes occurring before Plinian eruptions of Popocatepetl volcano. In *Insights from textural-compositional variations in plagioclase and Sr-Nd-Pb isotopes* (Vol. 167, pp. 1–19). Contributions to Mineralogy and Petrology. https://doi.org/10.1007/s00410-014-0966-x

Sosa-Ceballos, G., Gardner, J. E., Siebe, C., & Macías, J. L. (2012). A caldera forming eruption ∼14, 10014 Cyr BP at Popocatépetl Volcano, México: Insights from eruption dynamics and magma mixing. *Journal of Volcanology and Geothermal Research*, *213–214*, 27–40. https://doi.org/10.1016/j.jvolgeores.2011.11.001

Vahle, C., & Kontny, A. (2005). The use of field dependence of AC susceptibility for the interpretation of magnetic mineralogy and magnetic fabrics in the HSDP-2 basalts, Hawaii. *Earth and Planetary Science Letters*, *238*(1–2), 110–129. https://doi.org/10.1016/j.epsl.2005.07.010

Wang, D., & Van der Voo, R. (2004). The hysteresis properties of multidomain magnetite and titanomagnetite/titanomaghemite in midocean ridge basalts. *Earth and Planetary Science Letters*, *220*(1–2), 175–184. https://doi.org/10.1016/S0012-821X(04)00052-4

Wooster, M. J., Kaneko, T., Nakada, S., & Shimizu, H. (2000). Discrimination of lava dome activity styles using satellite-derived thermal structures. *Journal of Volcanology and Geothermal Research*, *102*(1–2), 97–118. https://doi.org/10.1016/S0377-0273(00)00183-9

Yamamoto, T., Takarada, S., & Suto, S. (1993). Pyroclastic flows from the 1991 eruption of Unzen volcano, Japan. *Bulletin of Volcanology*, *55*(3), 166–175. https://doi.org/10.1007/bf00301514